Electronic Supplementary Material (ESI) for Journal of Materials Chemistry C.

Supporting Information

Modulating Photoelectron Localization Degree to Achieve Controllable Photoluminescence Quenching and Activation of 0D Hybrid Antimony Perovskites

Dong-Yang Li,[a,b] Yu Cheng,[a] Yu-Han Hou,[a] Jun-Hua Song,[a] Chuan-Ju Sun,[a] Cheng-Yang Yue[a], Zhi-Hong Jing[b*] and Xiao-Wu Lei [a*]

[a] School of Chemistry, Chemical Engineer and Materials, Jining University, Qufu, Shandong, 273155, P. R. China

[b] School of Chemistry and Chemical Engineering, Qufu Normal University, Qufu, Shandong, 273165, P. R. China

Corresponding Authors: Zhi-Hong Jing; Xiao-Wu Lei

E-mail: zhhjing@126.com; xwlei_jnu@163.com

Table of Contents	
Fig. S1	The detailed arrangement structures of $[SbCl_5]^{2-}$ unit in $[BPP]SbCl_5$ and $[BPPP]SbCl_5$.
Fig. S2	The detailed coordination environments of $[SbCl_5]^{2-}$ unit in $[BPP]SbCl_5$ and $[BPPP]SbCl_5$.
Fig. S3	The simulated and experimental powder X-ray diffraction patterns of $[BPP]SbCl_5$ and $[BPPP]SbCl_5$ prepared from solution reaction.
Fig. S4	The SEM and elemental mapping images of $[BPPP]SbCl_5$ bulk crystal.
Fig. S5	The PLQY of $[BPPP]SbCl_5$ bulk crystal at 300 K.
Fig. S6	The emission wavelength dependent excitation spectrum and excitation wavelength dependent emission spectrum of $[BPPP]SbCl_5$ at 300 K.
Fig. S7	The consecutive 3D PL excitation and emission correlation maps of $[BPPP]SbCl_{5.}$
Fig. S8	The PL decay curve monitoring at 467 nm of $[BPPP]SbCl_5$ at 300K
Fig. S9	The PL emission spectrum and decay curve of $[BPPP]Cl_2$ at 300 K
Fig. S10	The comparison of powder X-ray diffraction patterns of bulk and microscale crystals of $[BPPP]SbCl_5$.
Fig. S11	Comparison of the SEM photos of bulk crystals and microscale crystals of $[BPPP]SbCl_5$.
Fig. S12	The entire Raman spectrum of $[BPPP]SbCl_5$ excited by 365 nm laser.
Fig. S13	The thermogravimetric analysis (TGA) curves of $[BPPP]SbCl_5$.
Fig. S14	The experimental PXRD patterns of $[BPPP]SbCl_5$ after constant heating at different temperature.
Fig. S15	The powder X-ray diffractions of $[BPPP]SbCl_5$ after soaking in various organic solutions over one day.
Fig. S16	The PL excitation and emission spectra of $[BPPP]SbCl_5$ after soaking in various organic solutions over one day.
Fig. S17	The powder X-ray diffractions of $[BPPP]SbCl_5$ after exposure in humid environment over 30 days.
Fig. S18	Comparison of PL emission spectra of $[BPPP]SbCl_5$ after exposure in humid environment over 30 days.
Fig. S19	White LED characterizations of $[BPPP]SbCl_{5.}$
Fig. S20	Normal characterizations of $[BPPP]SbCl_5$ based film.
Fig. S21	Anti-counterfeiting application of $[BPPP]SbCl_5$.
Fig. S22	The photo images of mechanical grinding process of $[BPPP]SbCl_5$ under the UV light irradiation.
Fig. S23	The simulated and experimental PXRD patterns of $[BPPP]SbCl_5$ prepared from solid phase grinding reaction.
Fig. S24	The PL emission spectrum of $[BPPP]SbCl_5$ prepared from solid phase grinding method.

Table S1	Summary of the photoluminescence properties of 0D antimony halide perovskite bulk crystals at about 300 K.
Table S2	Crystal Data and Structural Refinements for [BPP]$SbCl_5$ and [BPPP]$SbCl_5$.
Table S3	Selected bond lengths (Å) and bond angles (°) for [BPP]$SbCl_5$.
Table S4	Hydrogen bonds data for compound [BPP]$SbCl_5$.
Table S5	Selected bond lengths (Å) and bond angles (°) for [BPPP]$SbCl_5$.
Table S6	Hydrogen bonds data for compound [BPPP]$SbCl_5$.

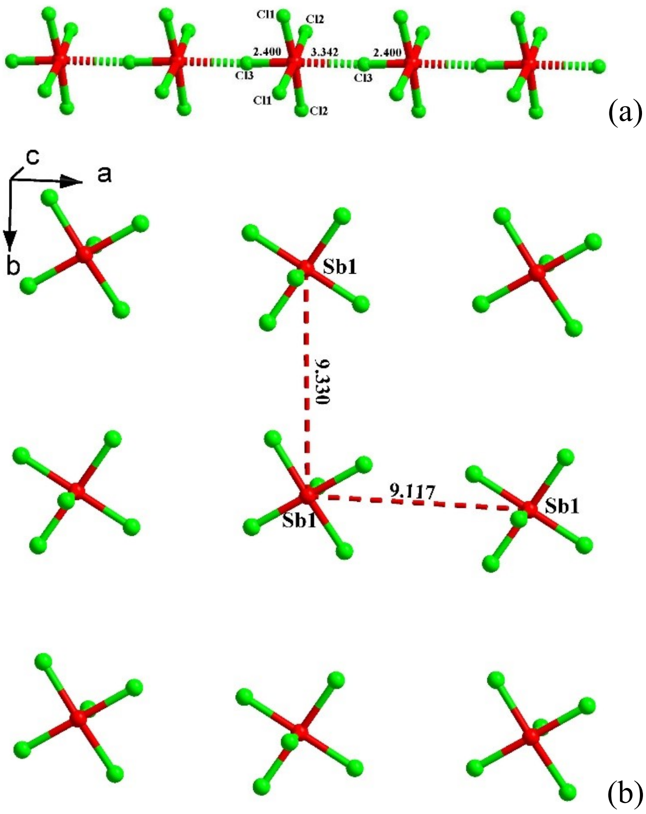

Fig. S1 The detailed arrangement structures of $[SbCl_5]^{2-}$ units in $[BPP]SbCl_5$ (a) and $[BPPP]SbCl_5$ (b).

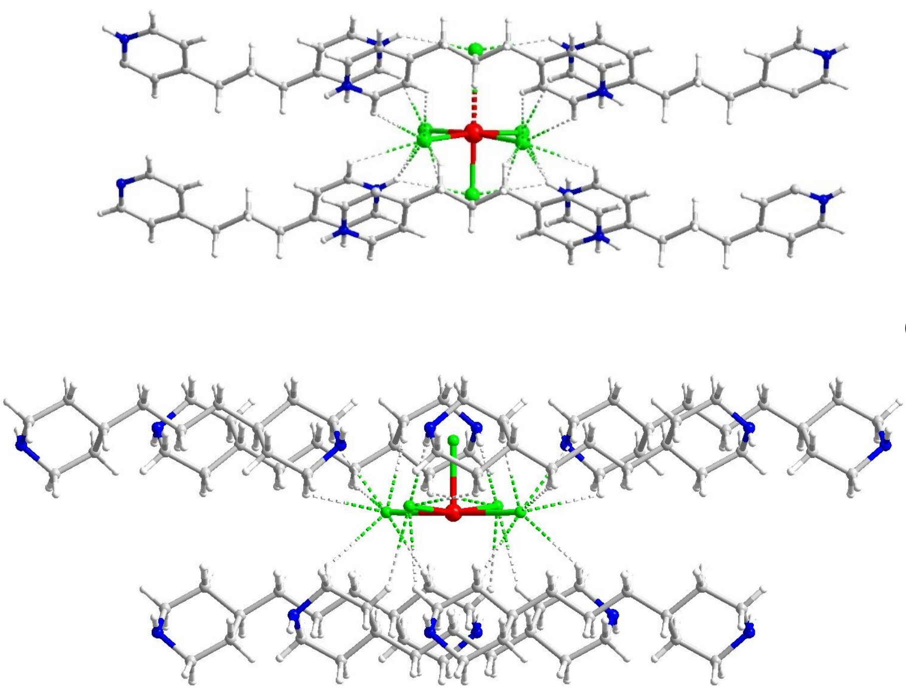

(a)

(b)

Fig. S2 The detailed coordination environments of $[SbCl_5]^{2-}$ units in $[BPP]SbCl_5$ (a) and $[BPPP]SbCl_5$ (b).

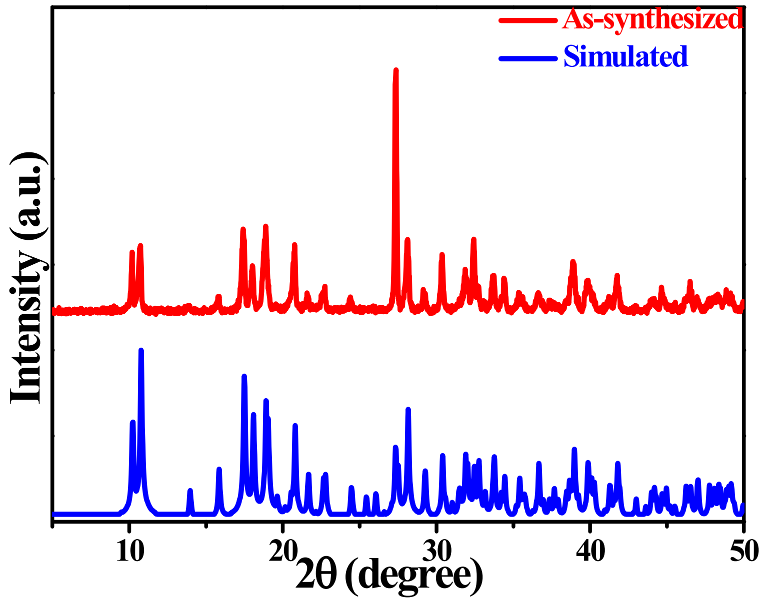

(a)

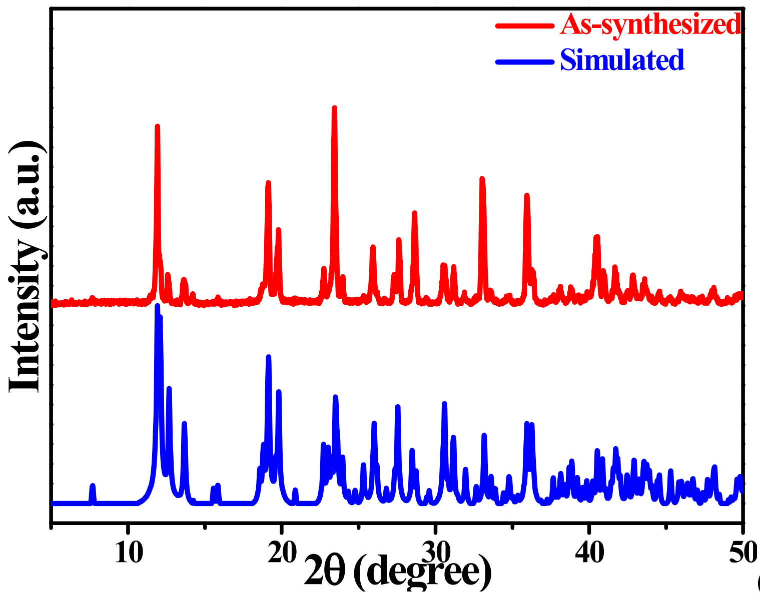

(b)

Fig. S3 The experimental and simulated PXRD patterns of [BPP]$SbCl_5$ (a) and [BPPP]$SbCl_5$ (b).

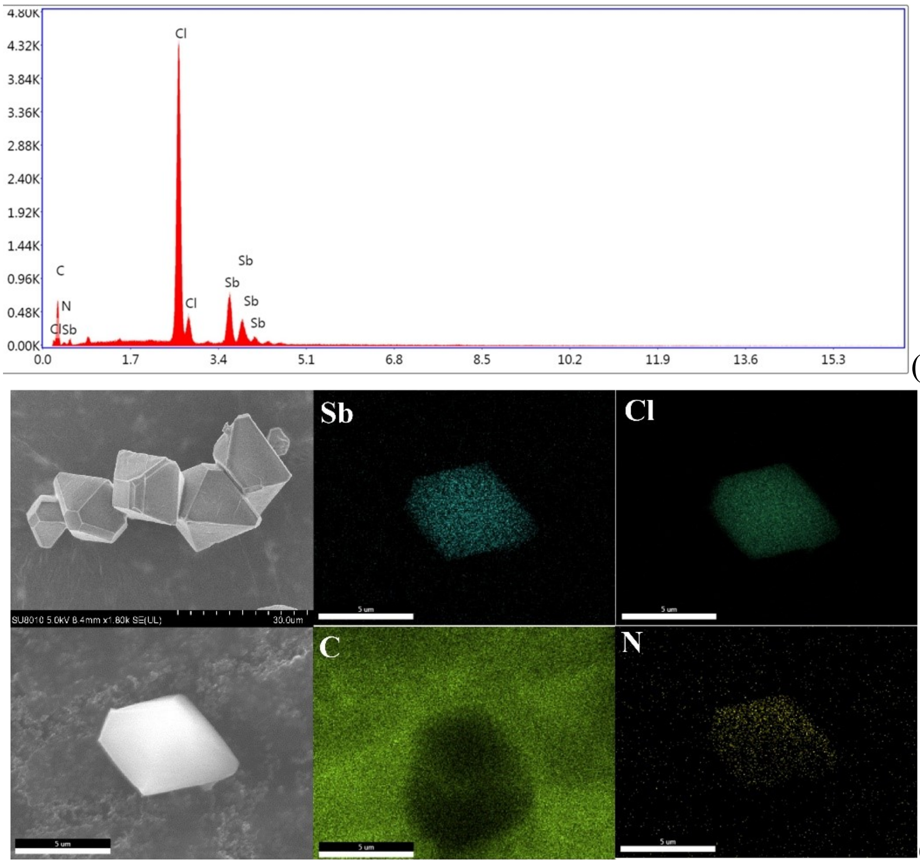

Fig. S4 The energy dispersive X-Ray spectroscopy (EDX) analysis result (a) and SEM and elemental mapping images (b) of [BPPP]$SbCl_5$ bulk crystal.

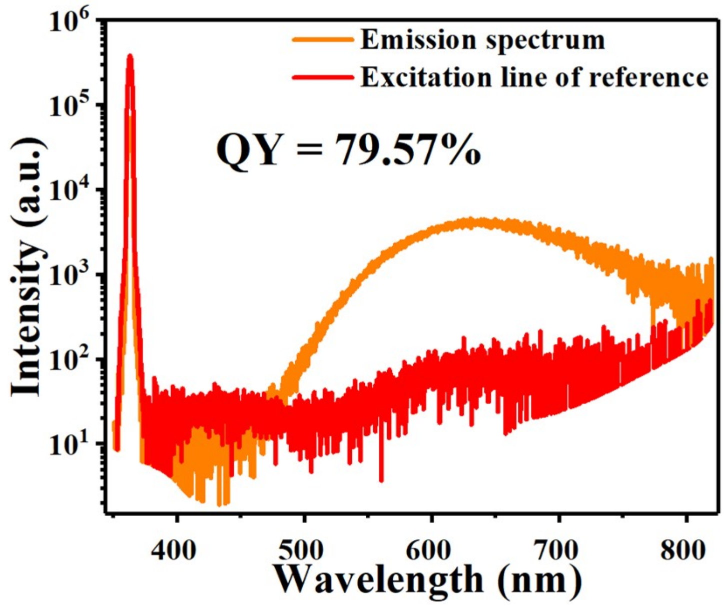

Fig. S5 The PLQY of bulk crystals for compound [BPPP]$SbCl_5$.

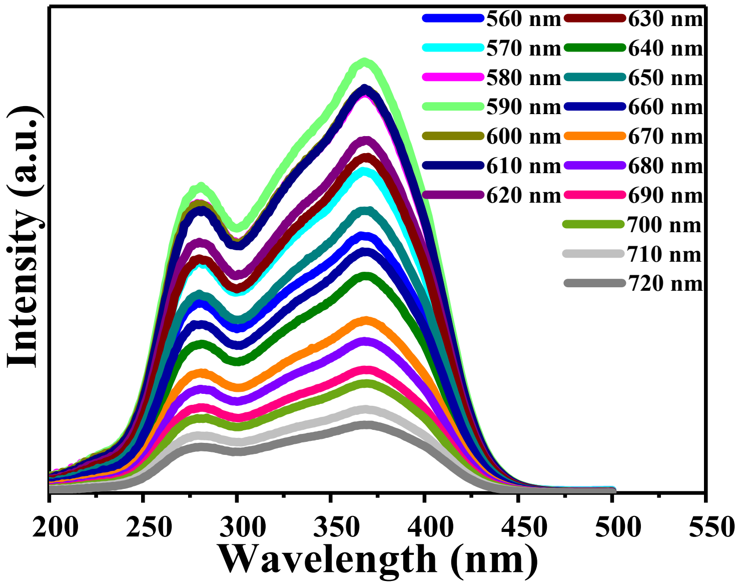

(a)

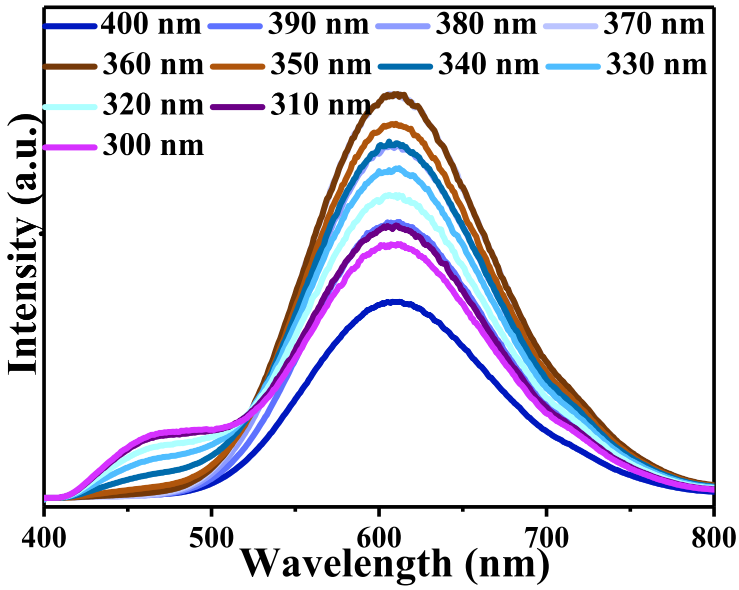

(b)

Fig. S6 The emission wavelength dependent PL excitation spectrum (a) and excitation wavelength dependent PL emission spectrum (b) of $[BPPP]SbCl_5$.

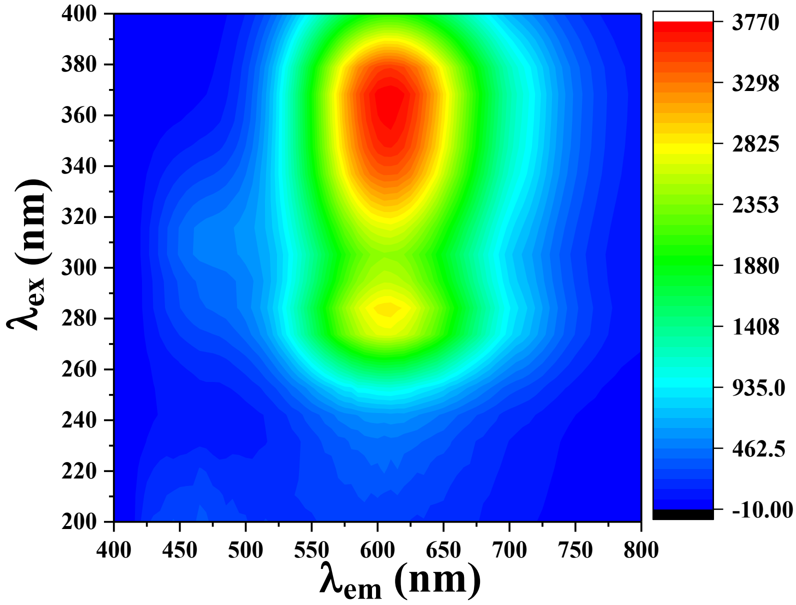

Fig. S7 The 3D consecutive PL excitation and emission correlation map of $[BPPP]SbCl_5$.

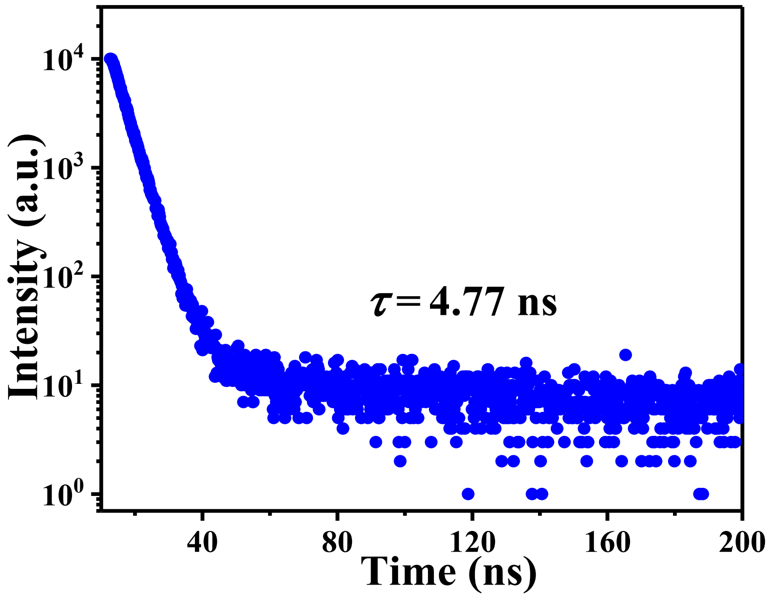

Fig. S8 The PL decay curve monitoring at 467 nm of [BPPP]$SbCl_5$ at 300 K.

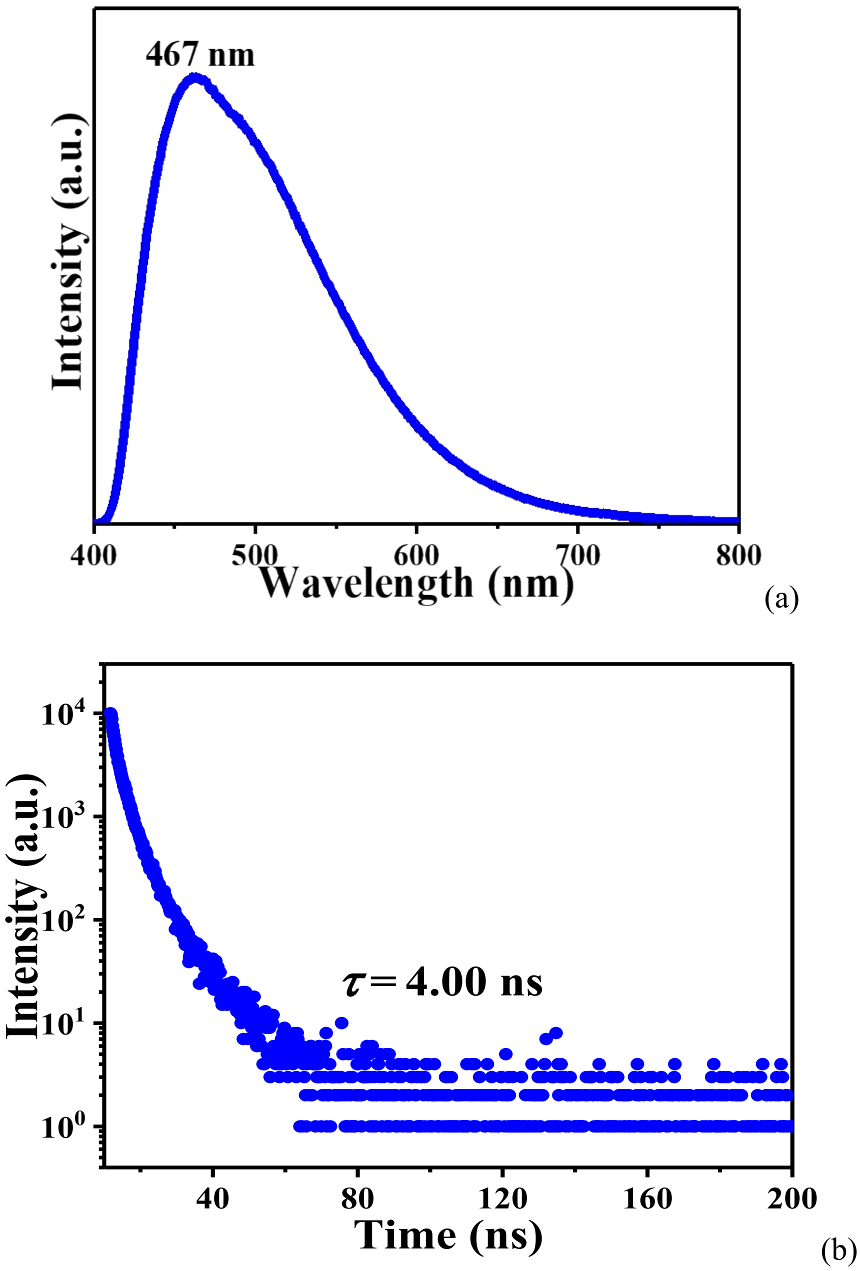

Fig. S9. The PL emission spectrum (a) and decay curve (b) of organic salt $[BPPP]Cl_2$ at 300 K.

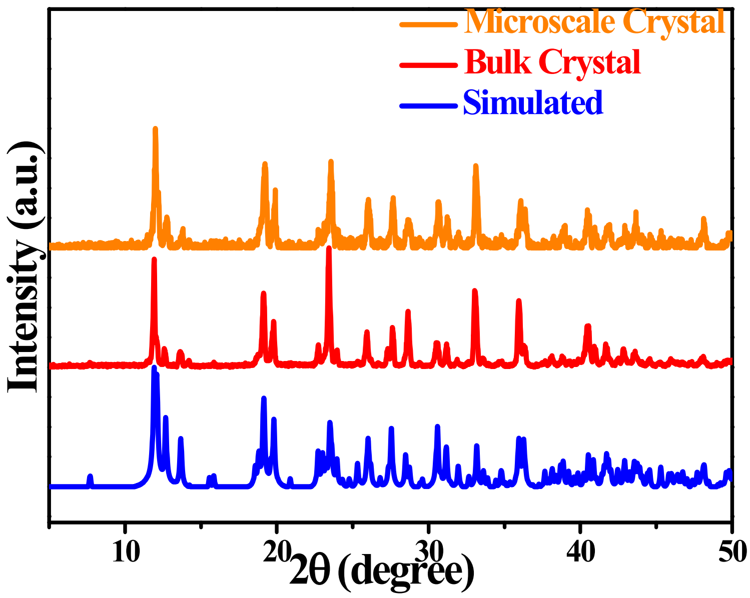

Fig. S10 Experimetnal PXRD patterns of bulk and microscale crystals as well as simulated data for $[BPPP]SbCl_5$.

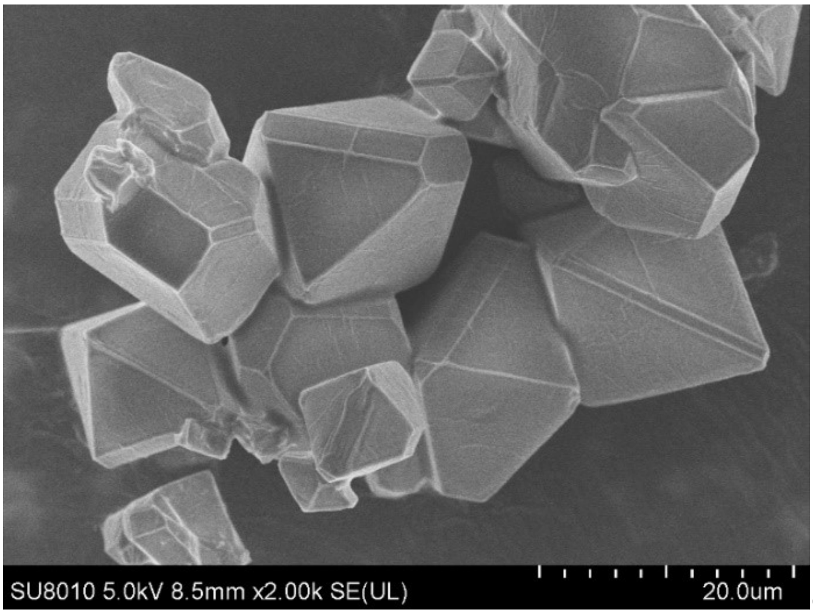

(a)

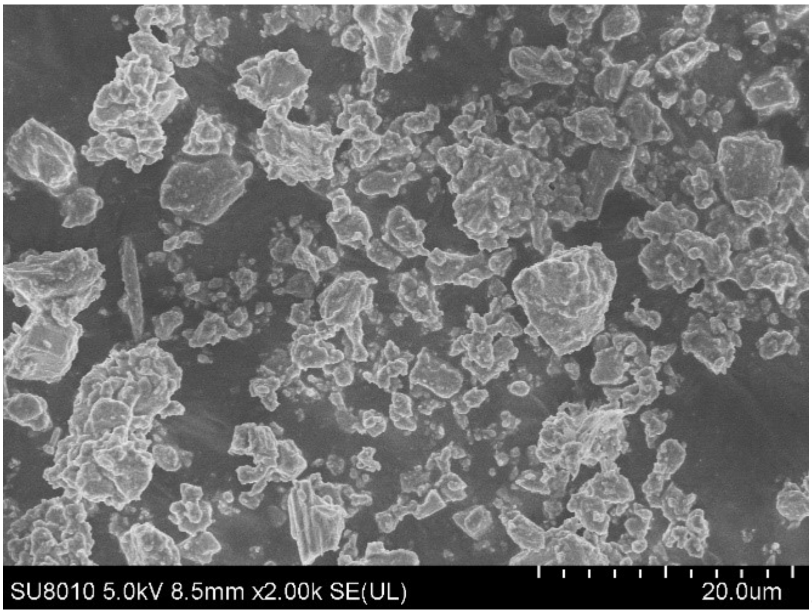

(b)

Fig. S11 The SEM photo images of bulk and microscale crystals of [BPPP]$SbCl_5$.

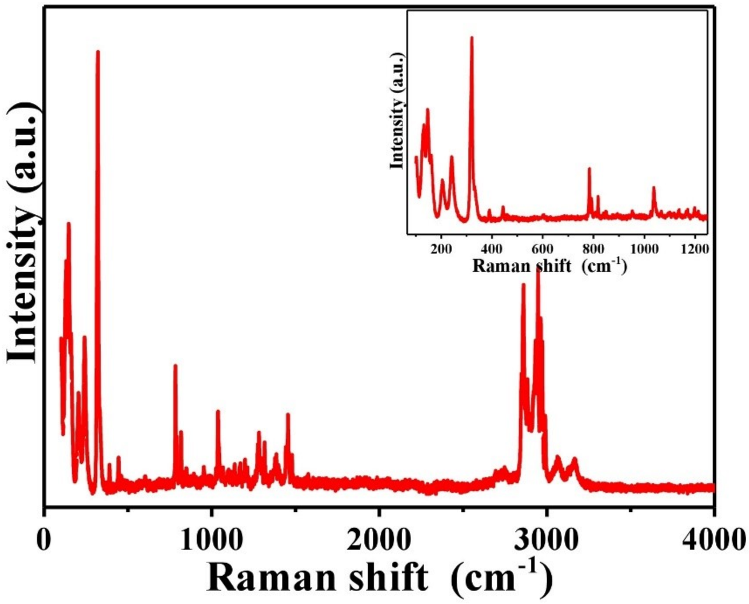

Fig. S12 The Raman spectrum of [BPPP]$SbCl_5$.

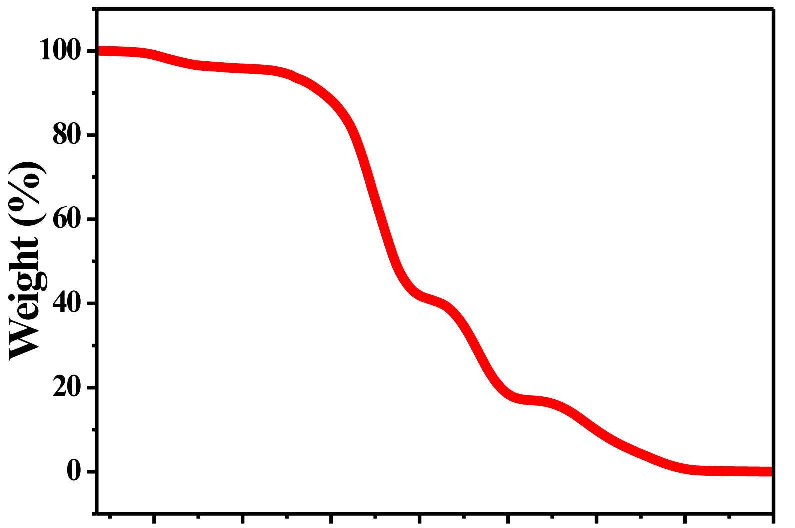

Fig. S13 The thermogravimetric analysis of [BPPP]$SbCl_5$.

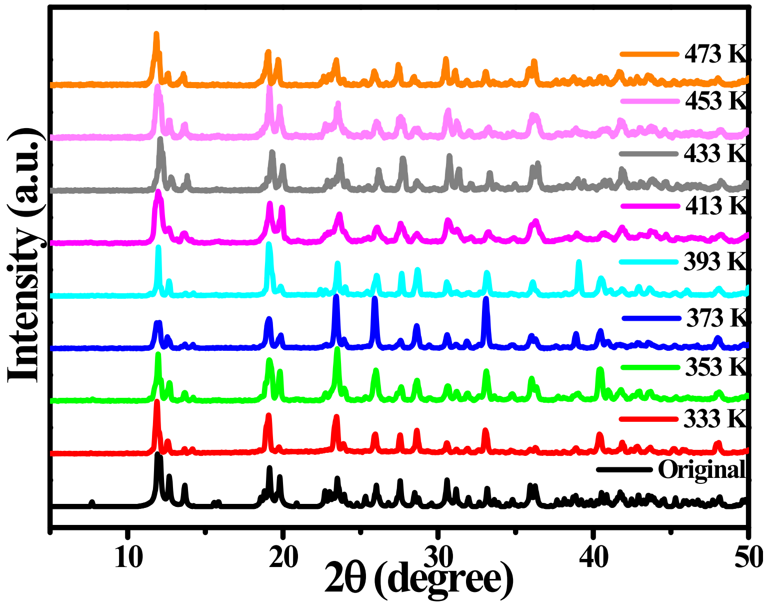

Fig. S14 The experimental PXRD patterns of $[BPPP]SbCl_5$ after constant heating at different temperature.

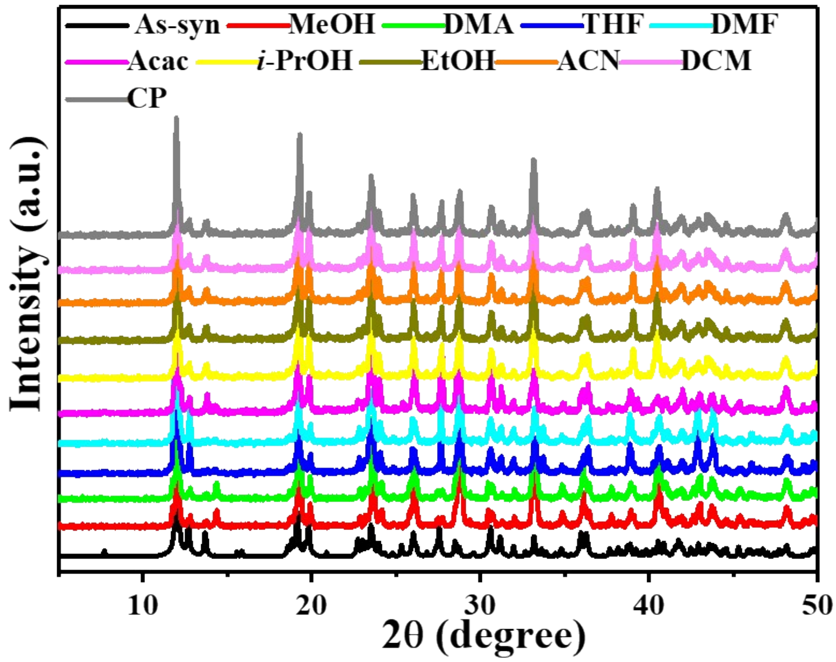

Fig. S15 The experimental PXRD patterns of $[BPPP]SbCl_5$ after soaking in various organic solvents over one day (DMA = N,N-Dimethylformamide,DMA = N,N-Dimethylacetamide, THF = Tetrahydrofuran, ACN = Acetonitrile, CP = Acetone, Acac= Acetylacetone, DCM= Dichloromethane).

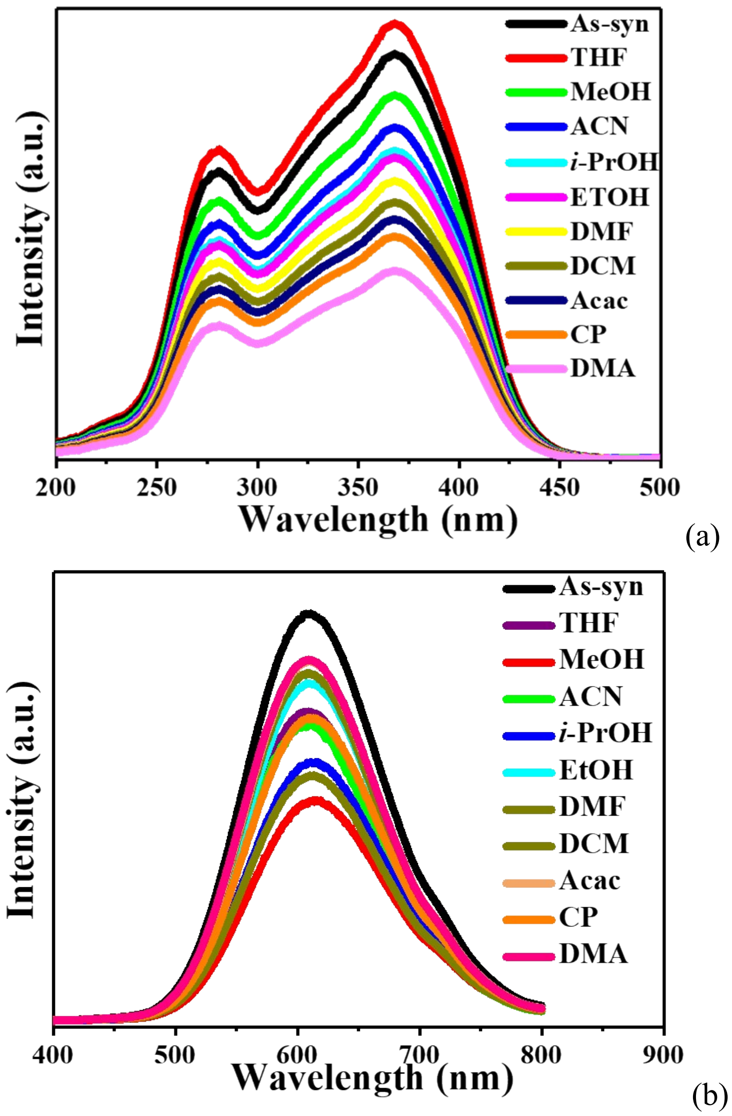

Fig. S16 The PL excitation (a) and emission (b) spectra of $[BPPP]SbCl_5$ after soaking in various organic solvents over one day (DMA = N,N-Dimethylformamide,DMA = N,N-Dimethylacetamide, THF = Tetrahydrofuran, ACN = Acetonitrile, CP = Acetone, Acac= Acetylacetone, DCM= Dichloromethane).

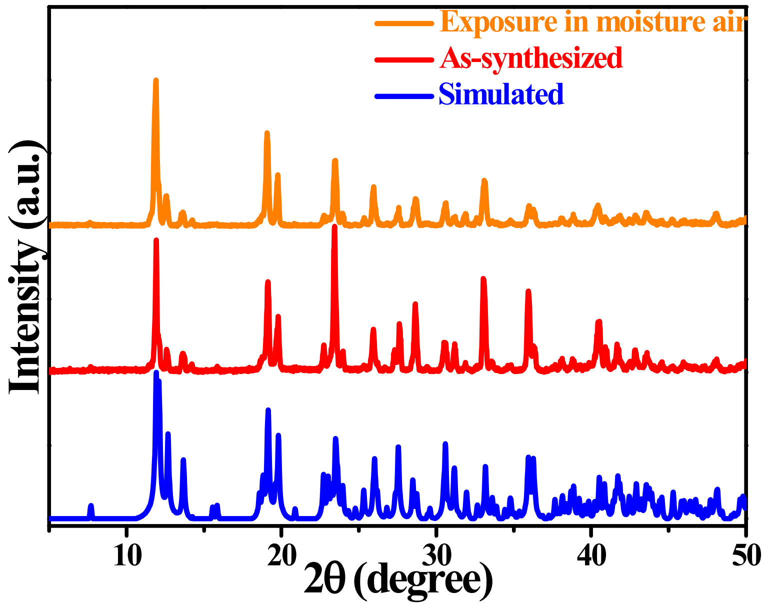

Fig. S17 The experimental PXRD patterns of [BPPP]$SbCl_5$ after storing in moisture air for one month.

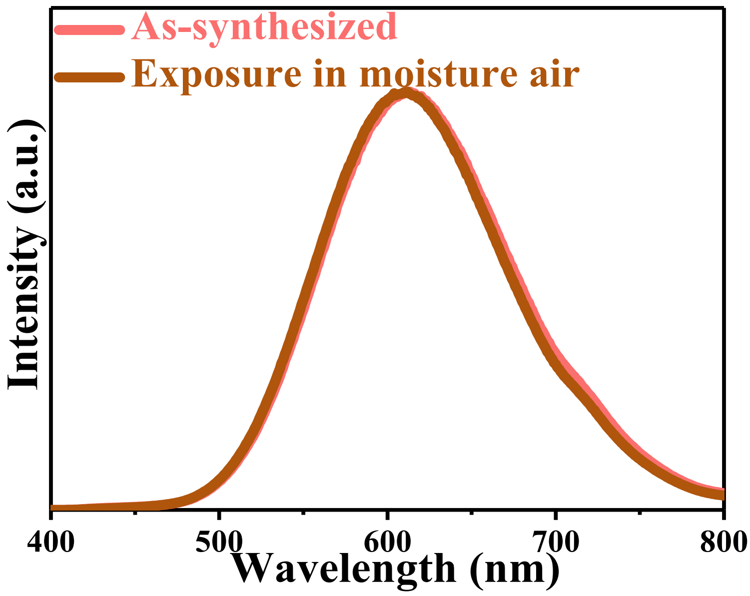

Fig. S18 Comparison of the PL emission spectra of [BPPP]$SbCl_5$ before and after storing in moisture air for one month.

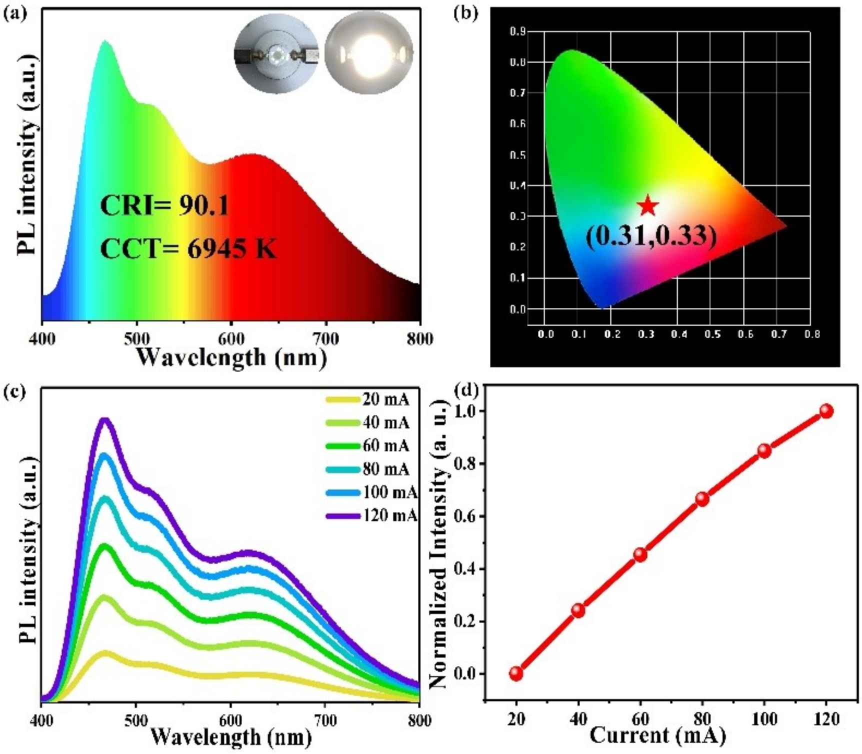

Fig. S19 Characterizations of white LED fabricated by yellow [BPPP]$SbCl_5$ phosphor and blue phosphor $BaMgAl_{10}O_{17}:Eu^{2+}$ on a UV chip: a) The PL emission spectrum at 20 mA drive current (inset: photographs of fabricated white LED before and after switching power supply); b) the CIE chromaticity coordinates; c) drive current dependent PL emission spectra; d) the normalized peak intensity variation under various operating currents.

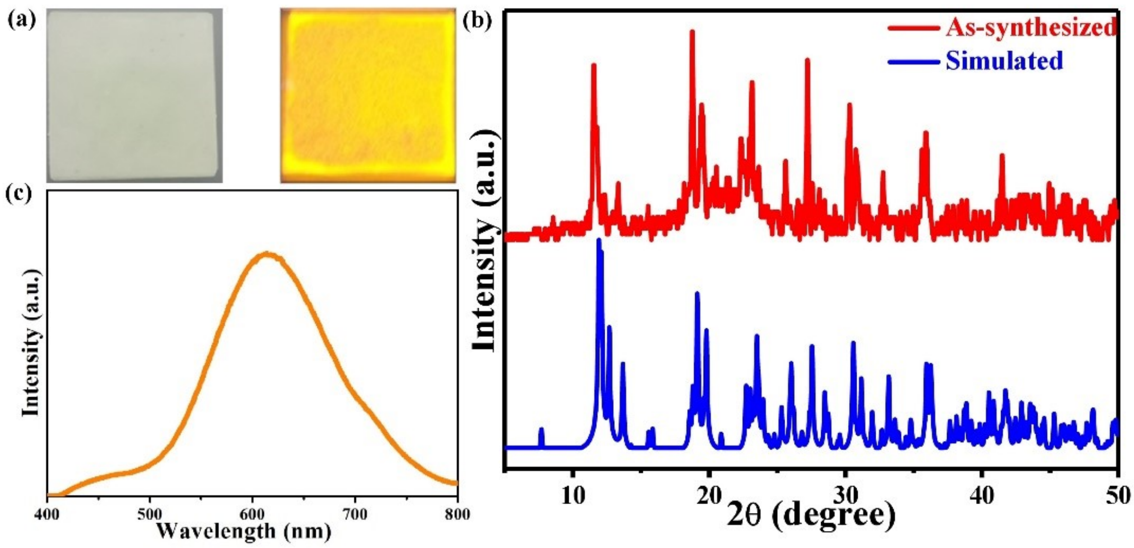

Fig. S20 Normal characterizations of [BPPP]$SbCl_5$ based film: (a) photographs under ambient light and 365 nm UV light, (b) experimental PXRD pattern and simulated data and (c) PL emission spectrum.

Fig. S21 Anti-counterfeiting application: the photo images of printed patterns by using luminescent $[BPPP]SbCl_5$ on commercial parchment paper under 365 nm UV lamp.

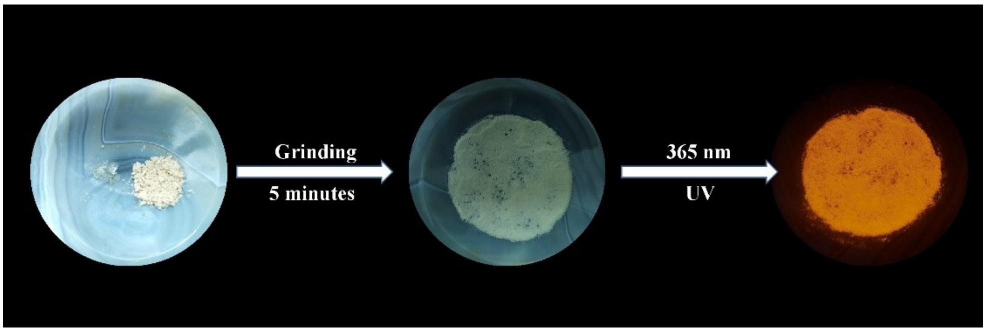

Fig. S22 The photo images of mechanical grinding process of [BPPP]$SbCl_5$ under the UV light irradiation.

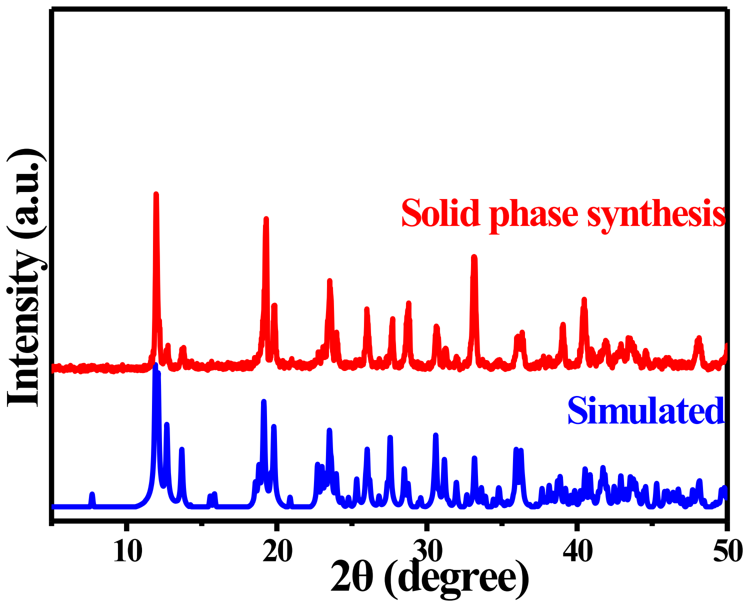

Fig. S23 The experimental PXRD patterns of [BPPP]$SbCl_5$ prepared form mechanical grinding solid-state reaction and simulated data from single crystal.

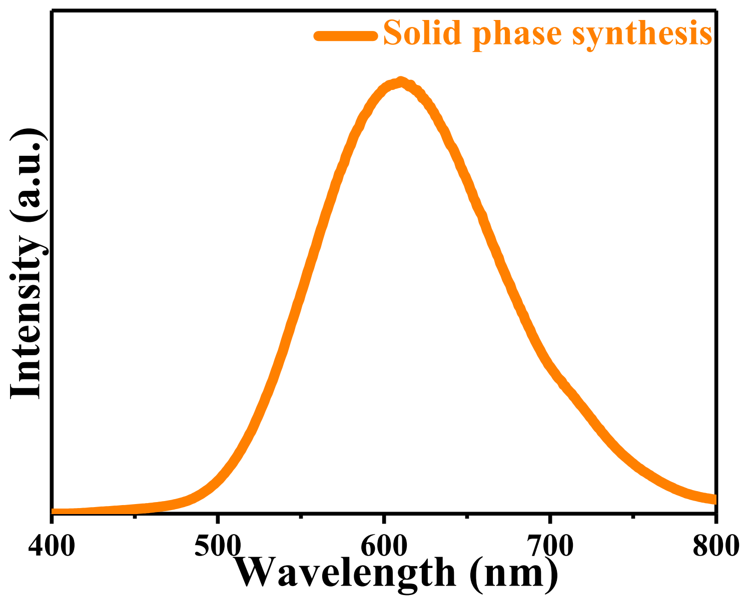

Fig. S24 The PL emission spectrum of [BPPP]$SbCl_5$ prepared form mechanical grinding solid-state reaction.

Table S1. Summary of the PL property 0D hybrid antimony halide perovskites.

Halides	λ_{em} nm	Stokes shift nm	FWHM nm	PLQY	Lifetime	Ref
			Square pyramidal [SbX_5] based halides			
$(PPN)_2SbCl_5$	635	225	142	98.1%	4.1 μs	1
$(TEBA)_2SbCl_5$	590	250	140	98%	13.44 μs	2
$(C_9NH_{20})_2SbCl_5$	590	210	119	98%	4.2 μs	3
$[C@Cs]_2SbCl_5$	664	320	149	89%	5.26 μs	4
$(Ph_4P)_2SbCl_5$	648	273	136	87%	4.75 μs	5
$[Bmim]_2SbCl_5$	583	215	....	86.3%	4.26 μs	6
$(TTA)_2SbCl_5$	625	250	140	86%	12.38 μs	1
$[BPPP]SbCl_5$	**610**	**242**	**131**	**79.5%**	**5.078 μs**	**This work**
$[C@Rb]_2SbCl_5$	686	346	165	75%	4.85μs	4
$[(NH_4)(18\text{-crown-6})]_2SbCl_5$	685	320	283	57%	3.8 μs	7
$[C@Rb]_2SbBr_5$	713	320	149	56%	2.28μs	4
$[Rb(18\text{-crown-6})]_2SbCl_5$	660	273	182	54%	5.4μs	7
$[TEMA]_2SbCl_5$	636	280	....	46%	....	8
$[Bzmim]_2SbCl_5$	600	225	....	22.3%	2.6 μs	9
$[(NH_4)(18\text{-crown-6})]_2SbBr_5$	735	292	198	....	1.4 μs	7
			Octahedral [SbX_6] based halides			
$[Bzmim]_3SbCl_6$	525	183	....	87.5%	2.4 μs	9
$[DMPZ]_2SbCl_6 \cdot Cl \cdot (H_2O)_2$	611	247	151	75.9%	2.336μs	10
$[H_3L_6]SbBr_6$	530	170	110	55%	2.15 μs	11
$[C@Ba]_4[SbBr_6]_2[Sb_2Br_8]$	591	206	137	46%	1.40 μs	4
$[C@Cs][C@Ba][SbBr_6]$	643	264	173	45%	1.28μs	4
$(H_3O)[TAEA]_2[SbCl_6] \cdot [Sb_2Cl_{10}] \cdot Cl_2$	517	165	110	45%	22.9μs	12
$[TAEA]_4[SbCl_6]_3 \cdot Cl_7$	580	200	140	43%	17.11μs	12
$[C@Rb][C@Ba][SbBr_6]$	617	241	155	40%	1.66μs	4
$[TAEA]_2(SbCl_6)_2 \cdot Cl_2$	638	290	160	6%	14.48μs	12

$(PEA)_4Bi_{0.57}Sb_{0.43}Br_7{\cdot}H_2O$	640	240	160	4.5%	0.234 μs	13
$Rb_7Sb_3Cl_{16}$	560	195	....	3.8%	0.2μs	14
$(PMA)_3SbBr_6$	625	200	175	<1%	1.508 ns	15

TTA = Tetraethylammonium; TEBA = Benzyltriethylammonium; PEA = phenethylamine, PPN = bis(triphenylphosphoranylidene)ammonium; DMPZ = N,N′-dimethylpiperazine; Bzmim = 1-benzyl-3-methylimidazolium; Bmim = 1-Butyl-3-methylimidazolium; L= 2-(3-methyl-1Himidazol-3-ium-1-yl)acetate; C_9NH_{20} = 1-butyl-1-methylpyrrolidinium; Ph_4P = tetraphenylphosphonium; 4-MP = 4-methylpiperidinium; $C_5N_2H_{16}$= N-ethyl-1,3-propanediamine; PMA = $C_6H_5CH_2NH_3$; TEMA = methyltriethylammonium; [C@M] = 18-crown-6 metal complex cation.

Table S2. Crystal Data and Structural Refinements for compounds [BPP]$SbCl_5$ and [BPPP]$SbCl_5$.

Compound	[BPP]$SbCl_5$	[BPPP]$SbCl_5$
chemical formula	$C_{13}N_2H_{16}SbCl_5$	$C_{13}N_2H_{28}SbCl_5$
fw	499.28	511.37
Temp (K)	273.15	293(2)
Space group	$P2_1/m$	Fddd
a (Å)	5.7073(2)	18.0893(3)
b (Å)	17.2780(6)	18.5179(4)
c (Å)	9.5155(4)	24.8339(4)
α (°)	90	90
β (°)	101.9505(10)	90
γ (°)	90	90
V(Å^3)	917.99(6)	8318.8(3)
Z	2	16
D_{calcd} (g·cm^{-3})	1.806	1.633
μ (mm^{-1})	2.224	16.393
F (000)	488	4096.0
Reflections collected	10855	6205
Unique reflections	2325	2066
GOF on F^2	1.084	1.083
$^aR_1,wR_2$ ($I > 2\sigma(I)$)	0.0138/0.0344	0.0277/0.0749
$^bR_1,wR_2$ (all data)	0.0146/0.0347	0.0307/0.0777

$^aR_1 = \sum||F_o| - |F_c||/\sum|F_o|$. $^bwR_2 = [\sum w(F_o^2 - F_c^2)^2/\sum w(F_o^2)^2]^{1/2}$.

Table S3. Selected bond lengths (Å) and bond angles (°) for compound [BPP]$SbCl_5$.

Sb1-Cl1	2.5556(4)	Sb1-Cl2[1]	2.6765(4)
Sb1-Cl1[1]	2.5556(4)	Sb1-Cl3	2.4001(5)
Sb1-Cl2	2.6765(4)		
Cl1-Sb1-Cl1[1]	93.873(19)	Cl1[1]-Sb1-Cl2[1]	87.515(14)
Cl3-Sb1-Cl2	86.279(15)	Cl1-Sb1-Cl2	87.516(14)
Cl3-Sb1-Cl2[1]	86.279(15)	Cl1[1]-Sb1-Cl2	174.462(14)
Cl3-Sb1-Cl1[1]	88.400(15)	Cl2[1]-Sb1-Cl2	90.608(18)
Cl1-Sb1-Cl2[1]	174.462(14)	Cl3-Sb1-Cl1	88.400(15)

[1]+X,1/2-Y,+Z

Table S4. Hydrogen bonds data for compound [BPP]$SbCl_5$.

D-H···A	d(D-H)	d(H···A)	d(D···A)	<(DHA)
N(1)-H(1A)···Cl(2)	0.84(2)	2.45(2)	3.165(17)	144.5(19)

Table S5. Selected bond lengths (Å) and bond angles (°) for compound [BPPP]$SbCl_5$.

Sb1-Cl1	2.3901(11)	Sb1-Cl3	2.5899(7)
Sb1-Cl2	2.6342(8)	Sb1-Cl3[1]	2.5899(7)
Sb1-Cl2[1]	2.6342(8)		
Cl1-Sb1-Cl2[1]	85.240(19)	Cl2-Sb1-Cl2[1]	170.48(4)
Cl1-Sb1-Cl3	89.642 (17)	Cl3[1]-Sb1-Cl2[1]	92.87(2)
Cl1-Sb1-Cl3[1]	89.642 (17)	Cl3-Sb1-Cl2[1]	87.07(2)
Cl1-Sb1-Cl2	85.240(19)	Cl3[1]-Sb1-Cl2	87.07(2)
Cl3-Sb1-Cl3[1]	179.28(3)	Cl3-Sb-Cl2[1]	92.87(2)

[1]5/4-X,5/4-Y,+Z

Table S6. Hydrogen bonds data for compound [BPPP]$SbCl_5$.

D-H···A	d(D-H)	d(H···A)	d(D···A)	<(DHA)
N(1)-H(1A)···Cl(2)	0.93(4)	2.39(4)	3.258(3)	155(3)
N(1)-H(1B)···Cl(2)	0.96(4)	2.72(4)	3.441(3)	132(3)
N(1)-H(1B)···Cl(3)	0.96(4)	2.57(4)	3.323(3)	135(3)

References

1. Q. He, C. Zhou, L. Xu, S. Lee, X. Lin, J. Neu, M. Worku, M. Chaaban, B. W. Ma, *ACS. Mater. Lett.,* 2020, **2**, 633-638.
2. Z. Li, Y. Li, P. Liang, T. Zhou, L. Wang, R. J. Xie, *Chem. Mater.,* 2019, **31**, 9363-9371.
3. C. Zhou, H. Lin, Y. Tian, Z. Yuan, R. Clark, B. Chen, L. J. van de Burgt, J. C. Wang, Y. Zhou, K. Hanson, Q. J. Meisner, J. Neu, T. Besara, T. Siegrist, E. Lambers, P. Djurovich, B. Ma, *Chem. Sci.,* 2018, **9**, 586-593.
4. V. Morad, S. Yakunin, M. V. Kovalenko, *ACS Mater. Lett.,* 2020, **2**, 845-852.
5. C. Zhou, M. Worku, J. Neu, H. Lin, Y. Tian, S. Lee, Y. Zhou, D. Han, S. Chen, A. Hao, P. I. Djurovich, T. Siegrist, M. H. Du, B. Ma, *Chem. Mater.,* 2018, **30**, 2374-2378.
6. Z. P. Wang, J. Y. Wang, J. R. Li, M. L. Feng, G. D. Zou, X. Y. Huang, *Chem. Commun.,* 2015, **51**, 3094-3097.
7. J. Xu, S. Li, C. Qin, Z. Feng, Y. Du, *J. Phys. Chem. C,* 2020, **124**, 11625-11630.
8. Z. Wang, D. Xie, F. Zhang, J. Yu, X. Chen, C. P. Wong, *Sci. Adv.,* 2020, **6**, eabc2181.
9. Z. Wang, Z. Zhang, L. Tao, N. Shen, B. Hu, L. Gong, J. Li, X. Chen, X.-Y. Huang, *Angew. Chem. Int. Ed.,* 2019, **58**, 9974-9978.
10. J. Q. Zhao, M. Han, X. Zhao, Y. Ma, C. Jing, H. Pan, D. Li, C. Yue, X. W. Lei, *Adv. Opt. Mater.,* 2021, 2100556.
11. F. Lin, H. Wang, W. Liu, J. Li, *J. Mater. Chem. C.,* 2020, **8**, 7300-7303.
12. A. Biswas, R. Bakthavatsalam, B. P. Mali, V. Bahadur, C. Biswas, S. S. K. Raavi, R. G. Gonnade, J. Kundu, *J. Mater. Chem. C.,* 2021, **9**, 348-358.
13. R. Zhang, X. Mao, Y. Yang, S. Yang, W. Zhao, T. Wumaier, D. Wei, W. Deng, K. Han, *Angew. Chem. Int. Ed.,* 2019, **58**, 2725-2729.
14. B. M. Benin, K. M. McCall, M. Wörle, V. Morad, M. Aebli, S. Yakunin, Y. Shynkarenko, M. V. Kovalenko, *Angew. Chem. Int. Ed.,* 2020, **59**, 14490-14497.
15. A. Khan, A. Zeb, L. Li, W. Zhang, Z. Sun, Y. Wang, J. Luo, *J. Mater. Chem. C.*, 2018, **6**, 2801-2805.